The Time of Flight Cooker Plugin

L. D. Ice and R. L. Russell

September 25, 2013

Contents

1 Introduction **2**

2 Data Analysis Methods **2**
2.1 Event Reconstruction . . . 2
2.1.1 Hit Time and Position . . . 3
2.1.2 Energy deposition . . . 4
2.2 Cosmic Ray Analysis . . . 5
2.3 Coplanarity . . . 6
2.4 Efficiency Calculations . . . 7
2.4.1 Efficiencies from SiPM Counters . . . 7

3 Digitization Process **7**
3.1 Output of Propagation . . . 7
3.2 Digitization Procedure . . . 8
3.2.1 Discrimination Simulation . . . 9
3.2.2 MC Efficiency . . . 10
3.3 How to use the ToF digitization . . . 10

4 Calibrations **11**
4.1 Reference Time Estimate . . . 11
4.2 Speed of Light . . . 11
4.3 TDC Offsets . . . 14
4.3.1 Mean Time Offsets . . . 15
4.3.2 Global Offset . . . 16
4.3.3 PMT Relative Offsets . . . 17
4.3.4 Results for TDC offsets . . . 18
4.4 ADC Parameters . . . 20
4.4.1 Pedestals . . . 20
4.4.2 Gains . . . 21
4.4.3 Attenuation . . . 22
4.4.4 Thresholds . . . 23
4.4.5 f-factors . . . 23

5 Future Work **24**

1 Introduction

The purpose of this OLYMPUS internal report is to describe the current status the of the time of flight detector analysis and digitization plugin, `Det_ToF`, for the Cooker* Framework. Section 2 gives an overview of the basic analysis tools in the ToF plugin and how they are used in the `tof` recipe to process raw data files. Section 3 goes over the ToF digitization methods that take the output of the Monte Carlo propagation plugin and reconstruct it the same format as the raw data. Section 4 summarizes some of the studies and calibrations for the ToF detector that are used in the initialization of constants in `Det_ToF`. Finally, we look at the future work that can be done for the plugin.

All of source code for the methods used in the ToF plugin can be found in the OLYMPUS Git repository within `src/plugins/detector/ToF/src/`. These are sorted into files by topic: `Det_ToF.cpp` contains the main methods for event reconstruction discussed in section 2.1. `ToFDigitization.cpp` contains the methods for the detailed Monte Carlo ToF digitization covered in section 3. `ToFefficiency.cpp` has the extra methods needed for the two types of efficiency calculations discussed in section 2.4. `ToFvis.cpp` provides the methods for displaying ToF hits in the OLYMPUS event display. `ToFcosmics.cpp` has additional methods useful in various ToF analyses using cosmic data (section 2.2.) `ToFCoplanar.cpp` contains all of the methods needed for the work presented in section 2.3. `ToFpedestal.cpp`, `ToFtdcoffset.cpp`, and `ToFthresh.cpp` can all be used to extract the relevant values discussed in section 4. `ToFsetup.cpp` sets all of the values from the ToF `init` file for use in the `Det_ToF` plugin. This `init` file is located at `src/plugins/detector/ToF/init/ToF.xml`.

A large number of Cooker recipes use `Det_ToF` methods. The primary ToF-only analysis recipe is `recipes/tof.xml`. The primary ToF-only digitization recipe is `recipes/MC/ToFDigi.xml`. The other ToF-specific recipes are: `recipes/tofsipm.xml` (efficiencies with SiPMs, section 2.4.1), `recipes/tofeff.xml` (efficiencies using data, section 2.4, which will require tracking), `recipes/tof/tof_threshold_test.xml` (thresholds, section 4.4.4), `recipes/tof/tof_pedestal_factory.xml` (pedestals, section 4.4.1), and `recipes/tof/tof_cosmics.xml` (cosmic ray studies, section 2.2.) ToF analysis methods can be added to recipes easily by following these ToF-only recipes as examples.

2 Data Analysis Methods

2.1 Event Reconstruction

For each triggered event, the `ToF` branch in the raw root files contains a reference time and, for each PMT, ADC and TDC values. The ToF bars are indexed i = 0-17 on the left side of the detector and i = 18-35 on the right. The PMTs are indexed such that j = 0-17 and j = 18-35 are the top PMTs on the left and right sides respectively, and j = 36-53 and j = 54-71 are the bottom PMTs on these same sides respectively. The lower numbers correspond to more downstream positions.

The first step of the analysis is to select ToF bars where both the top and bottom PMTs have TDC values between channels 1000 and 3000. These ToF bars are considered to have valid particle hits in them and are fully analyzed.

*/ðə ˈkuːkər/

The main task of the analysis is to reconstruct from the raw data the mean time, vertical position along the bar, and energy deposition of a particle's interaction with the scintillator material.

2.1.1 Hit Time and Position

The mean time t^i (from the initial scattering event) and the hit position y^i (from the center of the bar) in ToF number i, are calculated as

$$t^i = \frac{1}{2}\left(\mathrm{TDC}\,{}^i_t + \mathrm{TDC}\,{}^i_b\right) t_{\mathrm{res}} \tag{1}$$

$$y^i = \frac{1}{2}\left(\mathrm{TDC}\,{}^i_t - \mathrm{TDC}\,{}^i_b\right) t_{\mathrm{res}} v^i_{\mathrm{sc}} \tag{2}$$

where $\mathrm{TDC}^i_{t(b)}$ is the corrected TDC value of the top(bottom) PMT of bar i. The TDC channel resolution, t_{res}, is currently set to 0.05 ns/channel. This was calibrated during BLAST and has yet to be redone for OLYMPUS. In the position calculation, v^i_{sc} is the speed of light in the scintillator material. Since the index of refraction in the scintillator material has changed over time, and not necessarily consistent between bars, the speed of light in each individual ToF bar must be determined. The procedure to do this is described in section 4.2.

The TDC values recorded in the raw data include a time offset from delays in the electronics, cables, and trigger. Hence, the raw TDC is related to the corrected TDC by

$$(\mathrm{TDC_{raw}})^i_{t(b)} = \mathrm{TDC}\,{}^i_{t(b)} + (\mathrm{TDC_{delay}})^i_{t(b)} + \mathrm{TDC_{ref}} \tag{3}$$

This total timing delay is different for each PMT and is determined by procedures outlined in section 4.3.

The calculated mean time, equation (1), then becomes

$$t^i = \frac{1}{2}\left[(\mathrm{TDC_{raw}})^i_t - (\mathrm{TDC_{delay}})^i_t + (\mathrm{TDC_{raw}})^i_b - (\mathrm{TDC_{delay}})^i_b - 2\times\mathrm{TDC_{ref}}\right] t_{\mathrm{res}} \tag{4}$$

As can be seen in Figure 1, the meantime distribution varies significantly for different types of hits, and thus can be used as part of a particle ID system.

The vertical position, equation (2), can also be written

$$y^i = \frac{1}{2}\left[(\mathrm{TDC_{raw}})^i_t - (\mathrm{TDC_{delay}})^i_t - (\mathrm{TDC_{raw}})^i_b + (\mathrm{TDC_{delay}})^i_b\right] t_{\mathrm{res}} v^i_{\mathrm{sc}} \tag{5}$$

Large differences in TDC times can cause positions to sometimes be reconstructed well outside of the physical ToF bar, as seen in Figure 2. However, for most hits, the reconstructed position is a good approximation of the actual hit position and agrees reasonably well with drift chamber data.

The reconstructed value y^i combined with the distance between the center of the target and the center of the ToF bar can be used to calculate the azimuthal angle of the particle. This can be used when looking for coplanar events with data just from the ToFs.

2.1.2 Energy deposition

With the top and bottom PMT ADC values, we would like to calculate the total energy deposited, E^i_{dep}, in a ToF bar hit. To achieve this, we use a simple model to relate the deposited energy to the raw ADC values produced from the two PMTs:

$$\text{ADC}\,^i_t = f^i\, G^i_t\, E^i_{\text{dep}}\, e^{\frac{y^i - L^i/2}{\ell^i}} + (\text{ADC}_{\text{ped}})^i_t \tag{6}$$

$$\text{ADC}\,^i_b = (1 - f^i) G^i_b\, E^i_{\text{dep}}\, e^{\frac{-y^i - L^i/2}{\ell^i}} + (\text{ADC}_{\text{ped}})^i_b \tag{7}$$

Here, f^i is the fraction of detected light seen by the top PMT for that event (see section 4.4.5.) The offsets $(ADC_{\text{ped}})^i_{t(b)}$ are described in section 4.4.1, and the PMT gains $G^i_{t(b)}$ in section 4.4.2. L^i is the length of the scintillator bar and ℓ^i represents the attenuation length in that bar. In our ToFs, the attenuation length is generally shorter than the bar length, so attenuation is a very significant effect. Section 4.4.3 discusses more of this important correction.

When both ADCs are good, the total energy deposition can then by estimated by combining (6) and (7) to average out f^i:

$$E^i_{\text{dep}} = \frac{1}{G^i_t}\left[\text{ADC}\,^i_t - (\text{ADC}_{\text{ped}})^i_t\right] e^{\frac{-y^i + L^i/2}{\ell^i}} + \frac{1}{G^i_b}\left[\text{ADC}\,^i_b - (\text{ADC}_{\text{ped}})^i_b\right] e^{\frac{y^i + L^i/2}{\ell^i}} \tag{8}$$

However, the ADC channels do not go above 9120, so some ADC values in otherwise good events fall into the overflow bin. In particular, lower energy protons, which lose a lot of energy in scintillator,

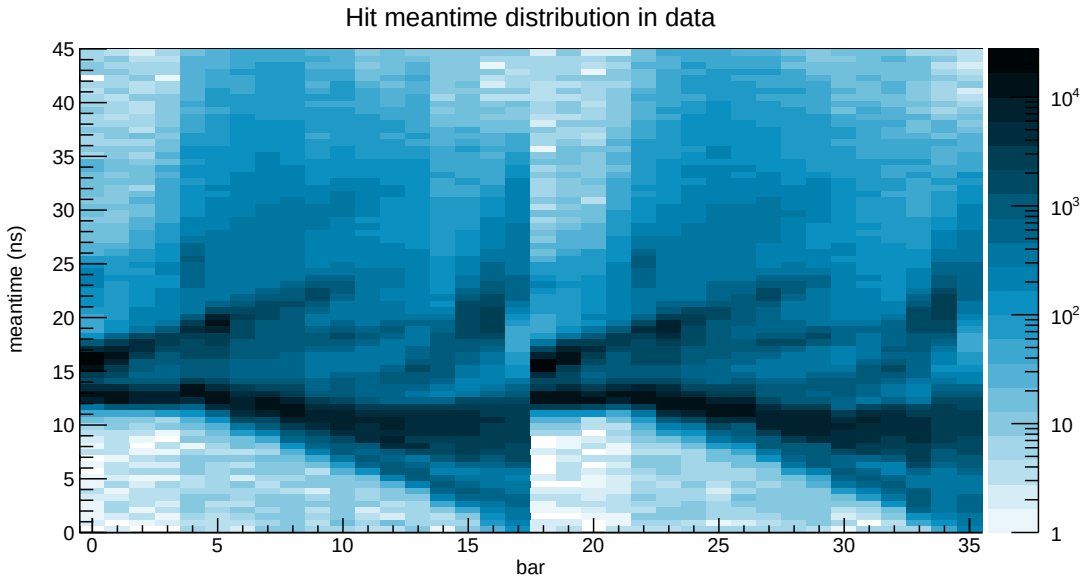

Figure 1: The meantime distribution for hits in a single regular data run, displaying a rich event structure. Elastic protons fall into the band that quickly increases in meantime in the back bars. Elastic leptons fall into the large band that has a constant meantime in the forward bars which decreases slowly in the back bars. The other bands arise from various background processes.

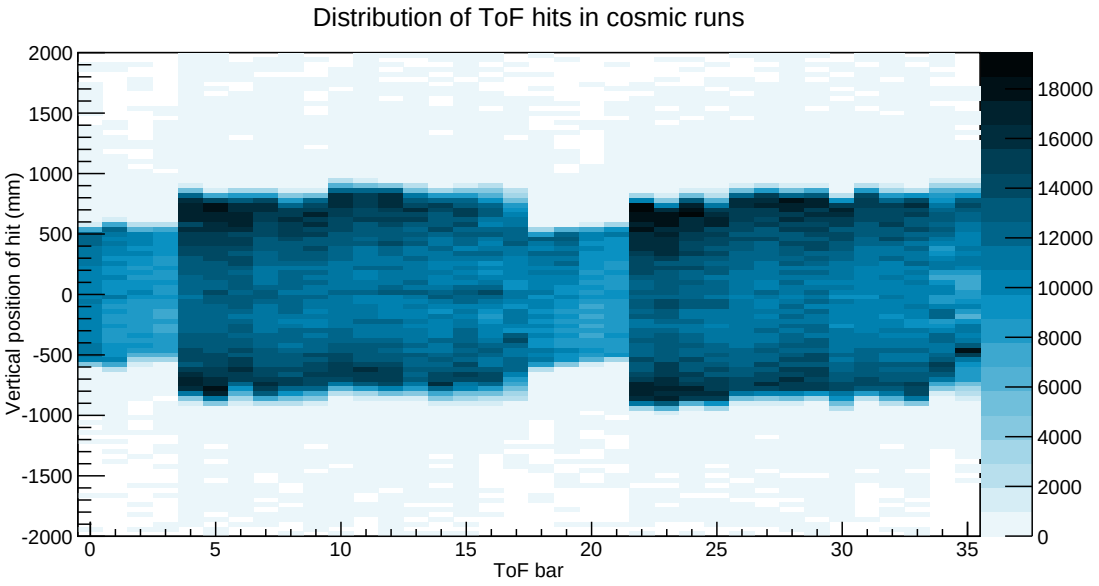

Figure 2: The distribution of reconstructed hit vertical positions (relative to bar centers) as a function of ToF bar for cosmic runs from January 2013. The four shorter forward bars can easily be seen in each side (left: 0-3, right: 18-21.) Hit positions in cosmic runs are biased to the top and bottom ends of the bars due to the angular distribution of cosmic rays.

can cause an ADC to overflow when they hit the bar close to one of the PMTs. In addition, some PMTs have high gains, which exacerbate this problem.

Ironically, the short attenuation lengths in our scintillator bars help us here, by protecting the PMT that is farther away from the hit position from being exposed to too much light. In regular data runs, nearly all hits in which one PMT has overflowed have a second good one. In cosmic runs, however, ADC overflows mostly come from vertical cosmic rays, which deposit enough energy to overflow both top and bottom PMT ADCs.

Thus, to calculate the energy deposition in hits with one overflowed ADC and one good ADC, we assume that $f^i = 0.5$ and calculate E_{dep} with just the good ADC. In other words, we assume that the light received by both PMTs, after correcting for attenuation, is equal. If the relative gains between the two PMTs are matched completely, this will be true on average. The error on the energy deposition calculated this way will be higher than when both ADCs are good by an amount known by the variation in f^i (see section 4.4.5.) When both ADCs in an event are overflowed, only a minimum energy deposition can be estimated.

2.2 Cosmic Ray Analysis

Much of what is described in the previous section is used directly for the cosmic ray analysis. The major difference is that the reference time is set to zero for cosmic ray runs. There are also specialized functions for cosmic rays in the `Det_ToF` plugin.

The first finds, using equation (1), the TDC mean time difference between bars on the left and right sides of the experiment. This mean time is corrected for the angle with respect to the horizontal that the cosmic rays travel between the bars. This has been used primarily to find

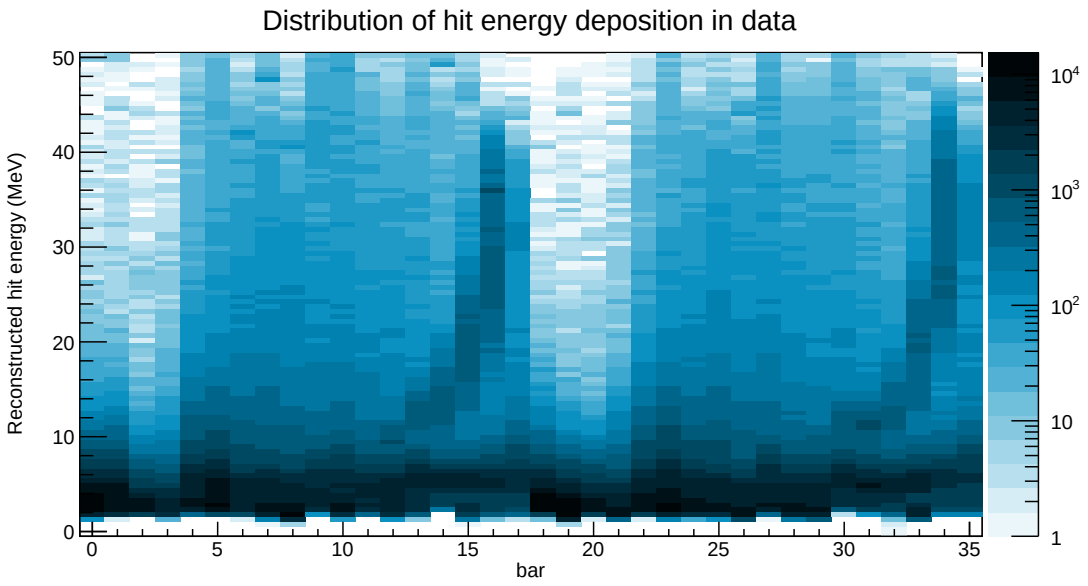

Figure 3: The distribution of reconstructed energy deposition for all events in a data run. Elastic protons fall into the dark band with increasingly high energy deposition in backwards ToF bars.

the relative TDC delay between bars (section 4.3) values. Another function creates a histogram of equation (5) divided by v_{sc}. This is for both the speed of light (section 4.2) study and determination of the relative TDC delay between pairs of PMTs.

Cosmic data also has use for ADC calibration (section 4.4.2.) Since cosmic muons are roughly minimally ionizing particles, almost all hits detected during cosmic runs will have similar dE/dx. To calculate the $d\text{ADC}/dx$ in a hit, it is important to know the path length of the muon within the scintillator. By using the reconstructed vertical positions for the two hits on opposite sides of the experiment along with geometrical information from the survey about the placements and angles of ToF bars, and assuming that all hits pass through the center of the bars, we estimate this path length fairly well. With tracking, even better path length corrections could be done since we would have some knowledge of the horizontal position of the hit in addition to the vertical position.

2.3 Coplanarity

For each ToF hit, the azimuthal angle, φ, is calculated from the y-position of the hit along the paddle and the distance from the center of the target cell to the center of the paddle. The φ angle for each ToF hit is saved in degrees from 0° to 360° with 0° along the positive x-axis. For each event, if the φ angles calculated from both hits are coplanar ±5° then the event is saved as being coplanar. The reason ±5° was chosen so that none of the elastic events would be improperly labeled as not coplanar and this is approximately the angular precision that can be achieved only using the time of flight detectors. The coplanarity functions also produce several histograms with more restrictive cuts to look for elastic events. Some of these include tighter cuts on coplanarity and cuts on timing differences between the hits. By making further coplanarity cuts, we are able to start to produce histograms that show the elastic peak from the data.

2.4 Efficiency Calculations

As the ToFs provide the primary trigger information for OLYMPUS, their acceptances and efficiencies dramatically affect the whole experiment. Thus, it is important to understand and measure these as fully as possible. Part of this is done using Monte Carlo to account for geometrical acceptance and inefficiency due to attenuation (section 3.2.2.) Some direct experimental measurements of efficiency can also be done.

The prescaled `0x9` (right ToF coincidence, left ToF either PMT) and `0x6` (left ToF coincidence, right ToF either) trigger patterns can be used to estimate the efficiency of each PMT in a way unbiased by the trigger. First, events with these trigger patterns are selected which have exactly one hit ToF bar and pattern match one drift chamber track in each sector. Then, for each PMT which is part of the ToF bar and is not guaranteed to have both TDCs valid by the trigger, the fraction of events that have a valid TDC if the other PMT's TDC is valid is found. This gives an efficiency for all 72 PMTs. These efficiency methods can be used by running the `tofeff` recipe.

2.4.1 Efficiencies from SiPM Counters

In January and February of 2013, cosmic runs were taken with SiPM sandwiches on the ToF bars using the `trigger12_toftest_sipm` trigger. Four SiPM sandwich counters were used at a time on adjacent ToF bars. For almost all runs, they were located on the center of the bars. Their bar positions for the corresponding run numbers are recorded in the ToF `init` file. ToF SiPM efficiencies can be calculated by running the `tofsipm` recipe. Three different efficiencies are recorded for each bar and SiPM system: the number of top PMT hits, the number of bottom PMT hits, and the number of coincidence hits, all divided by the number the SiPM sandwich counts. The coincidence efficiencies calculated over all runs are shown in Figure 4.

3 Digitization Process

3.1 Output of Propagation

In the new Monte Carlo structure, the propagation recipe produces a root file with minimal information for the digitization process. For each ToF bar hit in an MC event, the root file contains the following information:

- ToF detector hit
  - Integer: 0-17 (left) or 18-35 (right)
- Hit location (mm)
  - OLYMPUS world coordinates
  - ToF local coordinates
  - No position smearing
- Energy deposited (MeV)
- Timing (ns)
- Momentum (MeV/c)

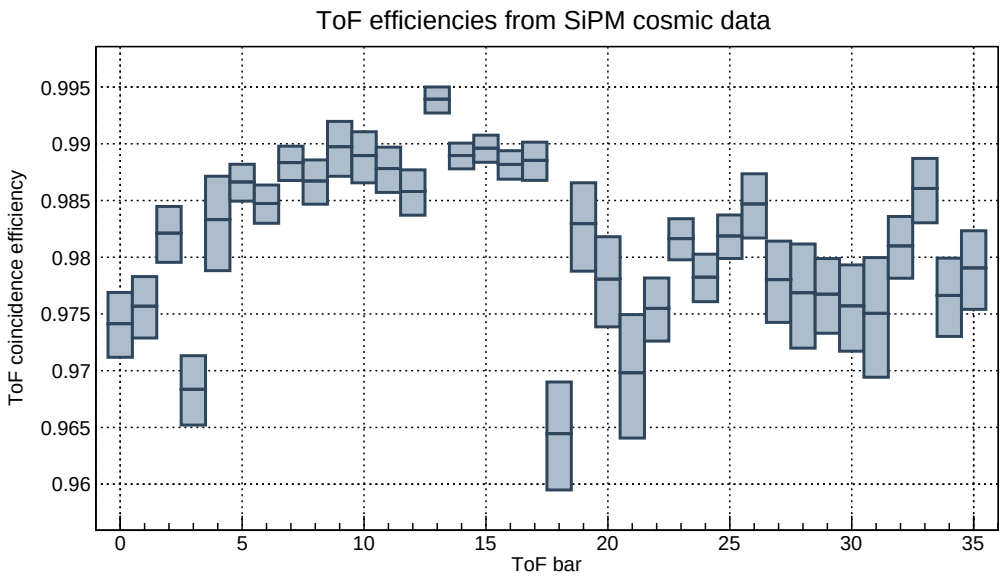

Figure 4: The top/bottom coincidence efficiency for each ToF bar generated from all 2013 cosmic SiPM ToF-test runs with SiPM sandwiches positioned in the center of the bars. These efficiencies provide an upper-bound on the ToF efficiencies since the relatively short attenuation lengths in our scintillator will cause the ends of the bars to be the least efficient regions.

- OLYMPUS world coordinates (4-momentum)
- ToF local coordinates

It is important to note that for each simulated track that traverses the ToF scintillator bar, there are multiple hits in the scintillator volume. All information saved in the root file is given per hit and is not the sum or average of the track over the scintillator volume.

3.2 Digitization Procedure

The purpose of the digitization is to take the simulated hits from the propagation root file and reproduce the same type of information that is in the raw data files – the ADC and TDC values and a reference time. Since the Geant4 MC propagation returns information for each step within each track in a detector volume, the digitization must take the potentially-large amount of information from all of the particles that traverse a bar of scintillator material and combine them. To do this, we try to follow what actually happens in the ToF detectors as much as possible.

First, an event reference time is generated from a Gaussian distribution with the appropriate width. Then, all hits within all tracks are placed into lists for the two PMTs on every bar. The energy at each PMT is appropriately reduced using the bar's attenuation length (section 4.4.3) and the local hit position. The time at each PMT is delayed using the bar's speed of light (section 4.2) and the local hit position. Then, the two hit lists are sorted by the local time at each PMT, which may change the ordering if there are multiple particle tracks in a bar or a steep track.

At this point, the energy smearing is applied to the pair of lists independently. The size of the smearing is determined on an event-by-event basis by first calculating the size of the f fluctuation,

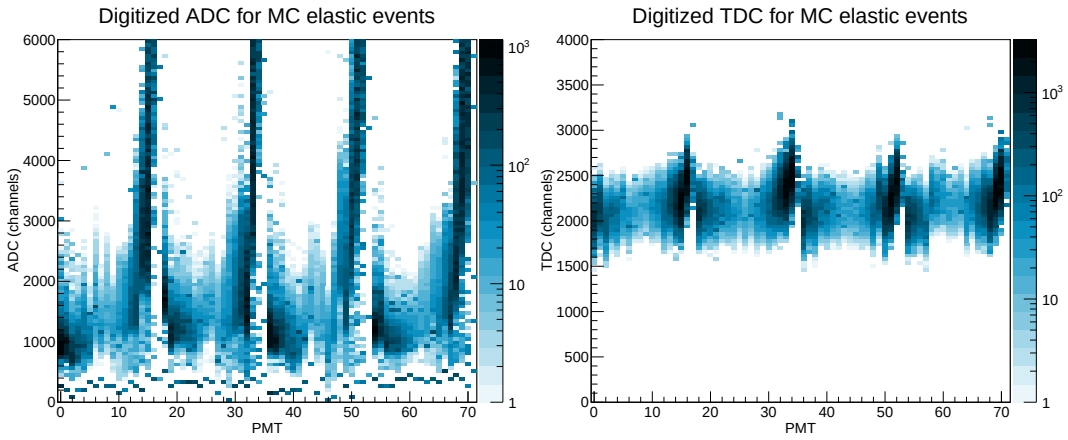

Figure 5: Simulated raw ADCs and TDCs for elastic events. Only values for PMTs on bars with nonzero deposited energy in an event are shown.

σ_f, at that total hit energy deposition (see section 4.4.5 for details) and then using the relation

$$\sigma^2 = 2E_{\text{dep}}^2\sigma_f^2 - \frac{1}{2}\left[(\sigma_{\text{noise}})_t^2 + (\sigma_{\text{noise}})_b^2\right] \tag{9}$$

where σ_{noise} is the electronic noise for a PMT that will be applied after the discrimination simulation. This relation ensures that we smear the correct amount such that we get the variation in f (section 4.4.5) that we observe in the data.

Next, each PMT hit list is sent to the `discriminate` method (section 3.2.1), which determines if and when the PMT registers a hit. If the PMT registers a hit, the ADC is calculated by summing all of the attenuated energies in its hit list, multiplying by the PMT gain (section 4.4.2), and adding the pedestal and some electronic noise (section 4.4.1.) If the value exceeds the maximum ADC channel, the ADC is set to the overflow bin. The TDC is calculated by converting the discrimination time to channels, adding the MC reference time, and subtracting the delay time for that PMT. Additionally, the time that it takes light to travel half the length of the ToF bar needs to be subtracted since this is implicitly included in the TDC offset.

This process results in ADC and TDC values like those found in the data, as can be seen in Figure 5, and a file that can be cooked with the `tof` recipe just like raw data files.

3.2.1 Discrimination Simulation

The `discriminate` method takes a list of attenuated and delayed hits at some PMT and determines if and when the threshold is passed for that PMT. There are two types of discriminators used for the ToFs. The vast majority of ToF PMTs use a constant fraction discriminator (CFD.) However, the back two ToF bars on each side use leading-edge discriminators, which can cause a TDC "walk" with signal size.

A hit signal in the ToF bar is modeled as a function of time by

$$A(t) = \frac{\alpha}{\tau_1 - \tau_2}\left(e^{-(t-t_0)/\tau_1} - e^{-(t-t_0)/\tau_2}\right)\theta(t - t_0) \tag{10}$$

where

$$\alpha \equiv \int_{-\infty}^{+\infty} A(t)\, dt \tag{11}$$

is proportional to the total amount of attenuated energy in the hit.

Here, τ_1 and τ_2 are both time constants arising from properties of the scintillator and PMT which roughly correspond to the decay time and the rise time of the signal, respectively. t_0 is the first time of arrival of the signal to the PMT and $\theta(t - t_0)$ is the Heaviside step function.

The values of τ_1 and τ_2 for our scintillator and PMT setups are not known. Instead, we have just estimated them with reasonable values. These are set in the ToF `init` file, and can be easily changed. In the ToF digitization initialization method, some important parameters are numerically computed with the `init` values: The single signal maximum amplitude, the time from t_0 at that maximum, and the minimum timing offset from a CFD with this signal.

The first step of the discrimination simulation is to produce a simple list of hits by combining hits that occur within the timing resolution of each other. This is purely for speed. When multiple signals reach a single PMT in one event, the total signal is just then modeled as the superposition of the corresponding versions of equation (10).

For the leading-edge discriminators, we just find the point at which the sum of the signals passes some threshold value and return that time. This is done numerically, extrapolating each exponential in time steps instead of repeatedly calculating exponentials.

Constant fraction discriminators split the signal, inverting and scaling one part, delaying the other part, then summing them again. The time of crossing at zero gives a time at constant fraction of the signal height. Unlike the leading-edge discriminator, this means that the timing offset for big signals and small amplitude signals with identical timing constants will be the same. The CFDs that OLYMPUS used have a scale of 0.3 and a delay of 10 ns. The same process that the CFD uses is simulated numerically. The time of zero crossing minus an offset that is equivalent to the delay between the zero crossing and the start of a signal for a single pulse signal is returned. When the signal is just one pulse, the initial time is simply returned.

3.2.2 MC Efficiency

Since the attenuation (section 4.4.3) in the ToFs is large, it can affect detection efficiencies significantly, and differently depending on the position and energy of the hit. Since the attenuation lengths and thresholds (section 4.4.4) can be extracted from data, Monte Carlo allows us to estimate how large this effect truly is. The detailed discrimination simulation should be a good estimate of how much the thresholds cut into weak signals. This efficiency is calculated by recording, for each PMT and vertical position along a ToF bar, the number of events that pass threshold according to the discrimination method divided by the number of events that deposit more than zero energy in the corresponding ToF bar. Some example results are shown in Figure 7.

3.3 How to use the ToF digitization

The digitization recipes can only be performed on root files produced by the MC propagation recipe. The MC is now in the same format as the analysis plugins and therefore have startup, process and finalize functions that need to be called in the recipe. The ToF digitization plugin also requires the slow control plugin. The ToF-only digitization can be run using the `MC/ToFDigi` recipe, and the full digitization – including the trigger digitization – can be run using the `MC/fullDigi` recipe.

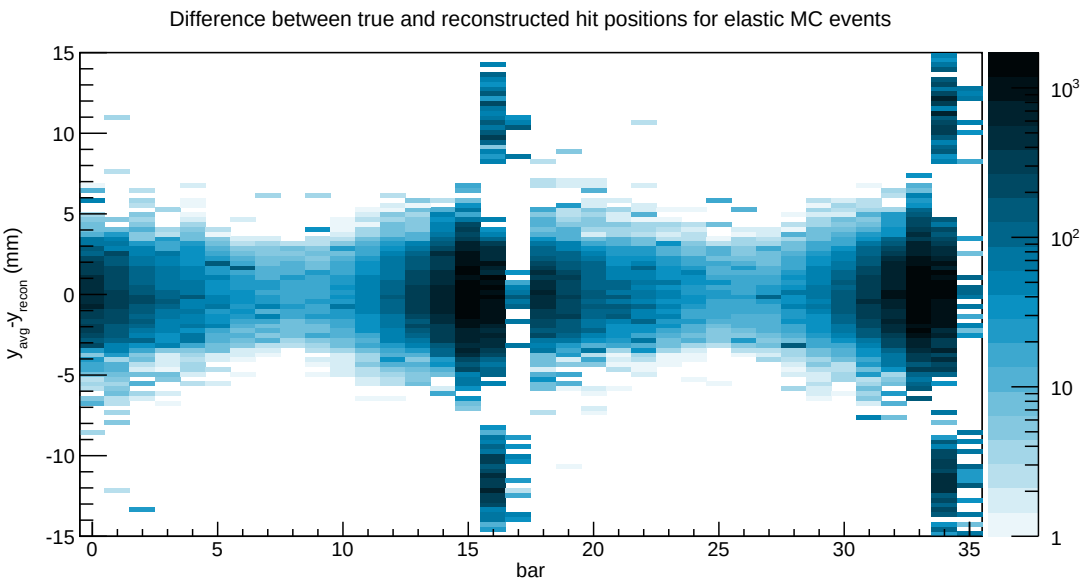

Figure 6: The quality of reconstructed hit positions in the MC for elastic events. The trigger simulation allows us to study interesting effects that arise from the interplay of signal shape and amplitude attenuation. For instance, the back two ToF bars on each side (16, 17, 34, 35), which are the ones with leading edge discriminators, tend to reconstruct the vertical hit position badly because of the "walk" of the attenuated signal.

4 Calibrations

4.1 Reference Time Estimate

To produce an accurate TDC offset for the ToF digitization process, a reasonable reference time must be included. The reference time for each MC event is chosen by drawing it randomly from a Gaussian distribution with a mean and standard deviation that corresponds closely to the reference time distribution from the data. To do this, the reference times for each data run were fitted with a Gaussian distribution and the mean and standard deviation were calculated. It was found that these two parameters varied for beam species and magnet polarity, but where fairly constant over the beam time except for several noticeable jumps. For each magnet polarity and beam species combination, the average mean and standard deviation were calculated for time periods where the parameters were fairly constant. The results were put into the ToF `init` file and are used by the digitization.

4.2 Speed of Light

The scintillator material used in the Time of Flight detector for OLYMPUS is Bicron BC-408 polyvinyl toluene with an index of refraction, n = 1.58 [1]. In an ideal situation, the speed of light, v_{sc} in the scintillator can be found from the index of refraction alone.

$$v_{sc} = c/n \tag{12}$$

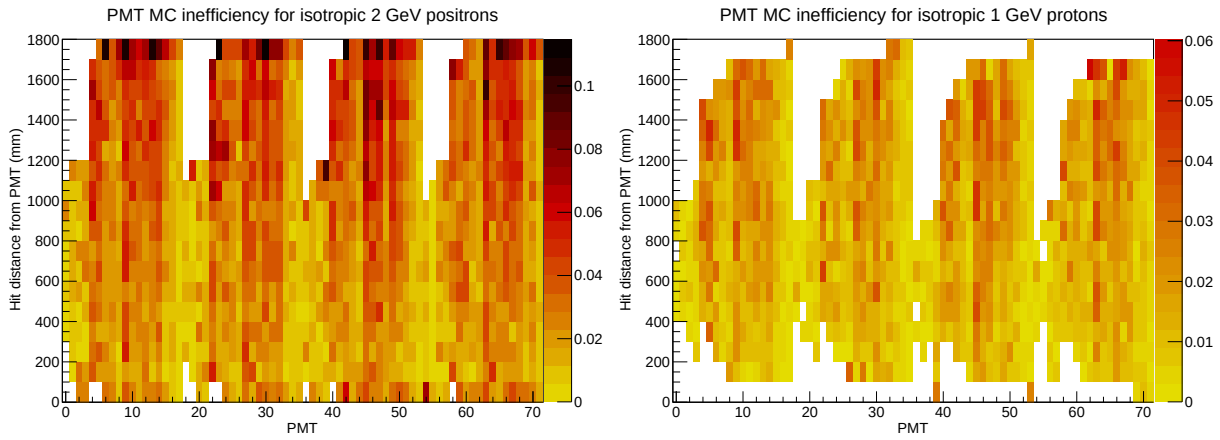

Figure 7: The inefficiencies for each PMT as a function of hit distance from that PMT, predicted by the Monte Carlo digitization. Bins in white are ones where statistics are too low to be displayed, or at positions that the scintillator does not reach to (for the shorter forward bars.) The left figure shows results for isotopic 2 GeV positrons from the target, and the right show results for isotropic 1 GeV protons from the target. Due to attenuation, the efficiencies farther from the PMT are lower. Since the protons deposit more energy in the scintillator, they have higher overall efficiencies.

Here c is the speed of light in a vacuum. In this case, the speed of light in the scintillators would be 189.74 mm/ns. Assuming that the time resolution of the photomultiplier tubes is 0.05 ns/channel, this gives the speed of light as 9.487 mm/channel.

As the scintillator ages and is exposed to radiation the index of refraction increases. Since the quoted index of refraction is no longer reliable, the current speed of light in the scintillators has to be obtained in an alternative way. This section describes a method to find the actual speed of light in the scintillator using cosmic ray data. This returns an average $v_{\text{sc}} = 6.98$ mm/channel, showing that the index of refraction has grown significantly over the years since the BLAST experiment began.

For each hit in the ToF detector, a TDC value from the PMT at either end of the scintillator material is recorded. The speed of light in the scintillator material can be found by measuring the TDC difference between the two PMTs for each hit. If the particle passes through the detector close to one of the PMTs, the TDC difference will be equal to the time it takes for the signal to traverse the whole length of the detector plus an unknown $\text{PMT}_{\text{offset}}$.

$$|\text{TDC}\,{}^{i}_{t} - \text{TDC}\,{}^{i}_{b}|_{\max} + (\text{PMT offset})^{i} = \frac{L^{i} t_{\text{res}}}{v^{i}_{\text{sc}}} \tag{13}$$

Here, L^i is the length of the detector (mm), t_{res} is the time resolution (ns/channel) and v_{sc} is the speed of light in the detector(mm/channel). The PMT offset can come from a difference in cable length or electronic delays and is discussed in section 4.3.3.

For each ToF detector $\text{TDC}\,{}^{i}_{t} - \text{TDC}\,{}^{i}_{b}$ is histogrammed over many cosmic ray events. This creates a Barad-dûr distribution [2] of width $\frac{2L^i}{v^i_{\text{sc}}}$ and centered around the PMT offset. An example of this is shown in Figure 8. Since L^i and t_{res} are known, this gives us a way to calculate the speed of light in the scintillator bars.

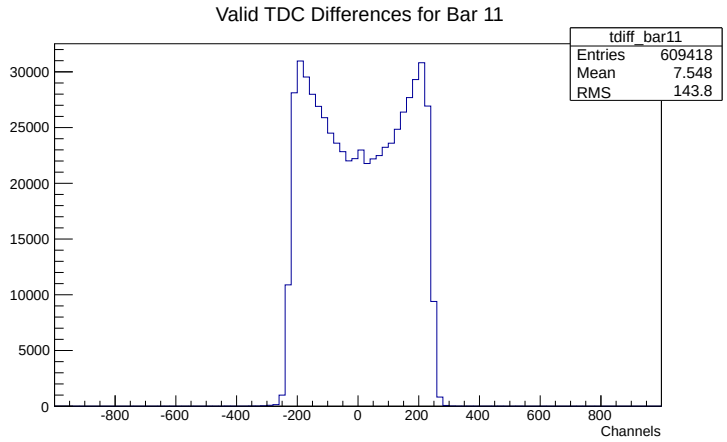

Figure 8: The TDC difference for many cosmic ray events in ToF 11.

Since the distribution was not quite square, the rise and fall of each distribution were fitted with a linear function and the x-intercept was used to calculate the width.

The benefit of using cosmic data instead of run-time data for this analysis, is that there is no shadowing at either end of the ToF detectors from the drift chamber frames. To get enough events to find the speed of light accurately, all the good cosmic ray data files from winter 2013 were used.

The resulting speed of flight for each scintillator bar are shown below in Table 1.

Left bar	v_{sc}(mm/channel)	Right bar	v_{sc} (mm/channel)
0	7.32	18	6.99
1	7.77	19	6.99
2	6.96	20	6.94
3	7.04	21	7.12
4	7.32	22	7.13
5	7.27	23	6.75
6	6.80	24	7.04
7	7.27	25	6.84
8	6.77	26	7.30
9	7.01	27	7.10
10	7.24	28	6.98
11	7.15	29	7.51
12	7.15	30	6.75
13	7.02	31	7.28
14	7.13	32	7.10
15	6.92	33	7.00
16	6.14	34	6.25
17	5.80	35	6.27

Table 1: Speed of light (mm/channel) for each of the time of flight detectors.

The values in table 1 are given in mm/channel. To find the speed of light in mm/ns, the values

in the table need to be divided by the PMT channel resolution t_{res}. If t_{res} is not the same for both PMTs on a detector, this calculation for the speed of light would not be valid.

There is evidence, however, that t_{res} is the same for both PMTs per bar. This evidence comes from looking at TDC_t^i vs TDC_b^i for each time of flight paddle. For many events with similar mean times, this should create a linear band with a negative slope. When this is done, it is found that the slope of TDC_t^i vs TDC_b^i is consistently approximately equal to -1, giving evidence that t_{res} is the same for both the bottom and top PMTs on a paddle. An example of this is shown in Figure 9 for ToF bar 11.

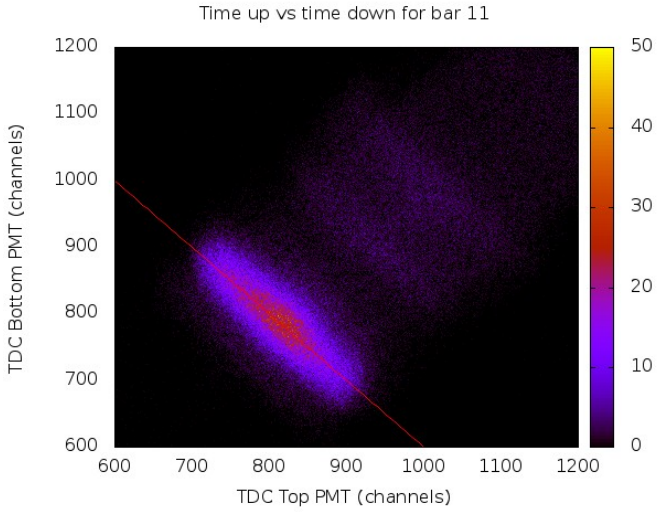

Figure 9: TDC_t^i vs TDC_b^i for ToF 11. The red line is linear with slope = -1 to show that t_{res} is the same for both PMTs

The speed of light in the scintillator bars has been measured using cosmic ray data and has been found to be close to 7 mm/channel. The actual values for the speed of light for each paddle is in the `Det_ToF init` file and is currently being used in the data analysis.

4.3 TDC Offsets

As seen in equations (3) and (5) the TDC values for each PMT includes delays from TDC electronics, cables, and trigger, and a reference time, TDC_{ref}, for each event.

Measuring the $(\text{TDC}_{\text{delay}})_{t(b)}^i$ per PMT is a difficult task and it is more straight forward to find a total offset for the mean time calculation and TDC delay difference for the hit position calculation. Once these have been found, they can be recombined to find $(\text{TDC}_{\text{delay}})_{t(b)}^i$.

The mean time offset was measured in two parts. The first is a offset for each paddle relative to the timing of the most forward left ToF (ToF 0). This relative mean time offset, r_{offset}^i, is the difference in calculated mean time equation (1) from delays per ToF, if a particle hit each paddle at the same time, t = 0.0ns for ToF 0. Since this offset only gives the relative offsets per paddle, it is missing a global offset, g_{offset} to move the calculated mean time to the actual time of flight of the particle. This relative offset per ToF and the global offset are defined in terms of the $(\text{TDC}_{\text{delay}})_{t(b)}^i$ per PMT.

$$r_{\text{offset}}^i - g_{\text{offset}} \equiv 0.5((\text{TDC}_{\text{delay}})_t^i + (\text{TDC}_{\text{delay}})_b^i)t_{\text{res}} \tag{14}$$

The relative mean time offsets are calibrated with a cosmic ray analysis is in section 4.3.1. The global offset, which is the same for all ToF bars, is calculated with Monte Carlo simulation in section 4.3.2.

The offset for the hit position calculation, PMT offset, is defined such that

$$(\text{PMT offsest})^i \equiv (\text{TDC}_{\text{delay}})^i_t - (\text{TDC}_{\text{delay}})^i_b \tag{15}$$

The PMT offsets were found using cosmic ray data. This procedure is described in section 4.3.3.

After the offsets, r^i_{offset}, $(\text{PMT offset})^i$ and g_{offset}, for each ToF paddle i, are found, they are combined to find a single offset per PMT.

4.3.1 Mean Time Offsets

To find the mean time offset for each ToF bar, we used cosmic ray events with coincident ToF hits in both the right and left sectors of the detector. By comparing the TDC mean time differences, $t^i_R - t^j_L$ for cosmic rays traveling left to right and right to left, corrected by the angle that the cosmic rays are passing through the detector, we were able to determine the absolute mean time calibration. The angle corrected mean time difference is given by

$$\frac{1}{2}\frac{(t^i_R - t^j_L)t_{\text{res}}}{\cos(\varphi)} \tag{16}$$

where t^i_R and t^j_L are the mean times for ToF detectors on the right (indexed by i) and left (indexed by j) respectively. The angle that the cosmic rays pass through the detector with respect to the horizontal is φ. When equation (16) is histogrammed for ToF bars i and j it produces a plot with two peaks; one for particles going left $\rightarrow$ right and another for particles right $\rightarrow$ left. The position of these two peaks is found by fitting them with Gaussian distributions and finding the peak positions. Labeling the positions of the two peaks L_{ij} and R_{ij} we then calculate S_{ij} as the difference between the left and right bar offsets.

$$\text{S}_{ij} = \frac{1}{2}(\text{L}_{ij} + \text{R}_{ij}) = (r_{\text{offset}})^i_R - (r_{\text{offset}})^j_L \tag{17}$$

Here, $(r_{\text{offset}})^i_R$ and $(r_{\text{offset}})^j_L$ are the mean time offsets for bars i and j. Since there are 18 ToF bars on either side of the detector, this results in $18\times18 = 324$ equations. The relative offsets are the solution to a least squares fit of these equations (17) weighted by $\sqrt{w_{ij}}$.

$$w_{ij} = \frac{1}{\left(\frac{\sigma^L_{ij}}{\sqrt{N^L_{ij}}}\right)^2 + \left(\frac{\sigma^R_{ij}}{\sqrt{N^R_{ij}}}\right)^2} \tag{18}$$

where $\sigma^{L(R)}_{ij}$ and $N^{L(R)}_{ij}$ are the standard deviation and integrated number of events in the Gaussian fit of the left(right) peak.

The least squares method returns the best solution for $(r_{\text{offset}})^i_L$ and $(r_{\text{offset}})^j_R$ for each ToF of flight detector relative to each other, up to an undetermined global offset. To account for this last undetermined offset, we set the left most forward ToF detector offset $(r_{\text{offset}})^0_L = 0$ with a very high weight. We then account for the undetermined global offset by adding a constant offset for all detectors described in section 4.3.2.

This procedure without the φ correction was done by Norik Akopov and this is presented at OLYMPUS Collaboration Meeting Feb. 25-26, 2013 → Report on ToF. A detailed description of the analysis done with the φ correction is located on the wiki under: detectors → Time of Flight Detector → ToF analysis → Cosmic Runs → ThetaCorrectedMeanTimeOffsets.

The results from the φ corrected analysis are shown in Table 2.

Left bar	$(r_{\text{offset}})_L$(ns)	Error(ns)	Right bar	$(r_{\text{offset}})_R$(ns)	Error(ns)
0	0	0.0000316	18	2.608	0.0073
1	5.2633	0.0073	19	4.2794	0.0073
2	-0.4456	0.0077	20	3.5466	0.0077
3	4.8185	0.0081	21	1.6033	0.0079
4	2.7205	0.0065	22	10.088	0.0063
5	5.9240	0.0062	23	8.5388	0.0063
6	2.6314	0.0067	24	8.3636	0.0064
7	6.1424	0.0064	25	6.6623	0.0066
8	4.9408	0.0069	26	3.8880	0.0065
9	5.9793	0.0065	27	7.8170	0.0065
10	4.3473	0.0065	28	1.2163	0.0064
11	7.0169	0.0064	29	7.6768	0.0062
12	2.7175	0.0064	30	4.5893	0.0065
13	8.7219	0.0066	31	6.9376	0.0062
14	2.0681	0.0066	32	5.6741	0.0065
15	2.8953	0.0068	33	8.2168	0.0066
16	12.1159	0.007	34	13.432	0.0092
17	11.0374	0.0086	35	15.455	0.0090

Table 2: Mean Time offsets(ns) for each of the time of flight detectors relative to ToF 0 (left most forward).

These mean time offsets are used in the calculation for the $(\text{TDC}_{\text{delay}})^i_{t(b)}$. A comparison of the offsets with and without the φ correction is shown in Figure 10 in section 4.3.2.

4.3.2 Global Offset

To include the global mean time offset for the ToF detectors a data-Monte Carlo comparison was done. In this study, the electron mean time in each ToF bar was found from the data and compared to Monte Carlo results. Using the old tracking code, tracks that were produced from an elastic electron-proton scattering event in the target region were selected. The calculated ToF mean time for these tracks was histogrammed for each ToF bar. To get enough statistics for this study, all of the February data with electron beam species and positive magnetic field polarity was used. Once there was enough statistics for every ToF bar, the electron mean time histogram was fitted with a Gaussian distribution and the peak position calculated.

The same study was then done with the Monte Carlo simulation, which returns the true interaction time with the detector.

The electron peak time from the data and Monte Carlo were compared and the last global offset

was introduced such that the data aligned with the Monte Carlo results. This comparison was done for each ToF bar and the offsets, g^i_{offset}, were found.

The offsets for each bar calculated using this method, compared favorably to the cosmic ray analysis in section 4.3.1. Since the cosmic ray analysis had better statistics, the results from that study were included in the ToF init file and are used for data analysis. The comparison of the mean time offsets is shown in Figure 10. The Monte Carlo simulation provided a global offset for all the ToF bars by taking g^0_{offset}, the general offset for ToF 0 and making this the global offset.

Because of the limited tracked data from the February run, this calibration needs to be redone after tracking is completed.

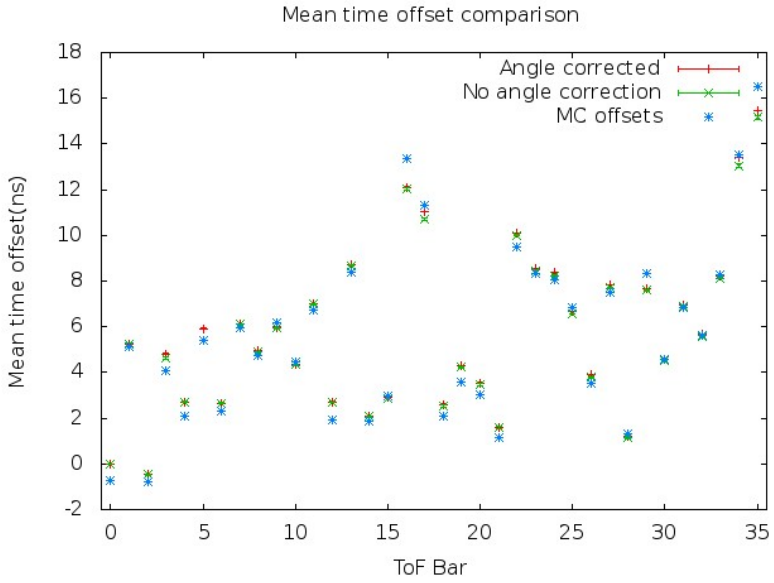

Figure 10: Comparison of mean time offset results. In red is the results the cosmic analysis with φ correction, green is from the cosmic analysis without φ correction and blue is the Monte Carlo results.

4.3.3 PMT Relative Offsets

The PMT relative offset for a bar is the difference between the TDC delay in the top PMT to the TDC delay in the bottom PMT as defined in equation (15). For this calibration the same procedure to find the speed of light (section 4.2) was used. For each ToF detector, the difference in the TDC values from the top and bottom PMTs $\text{TDC}^i_t - \text{TDC}^i_b$ is histogrammed over many cosmic ray events. This creates a distribution of width $\frac{2L}{v_{sc}}$ and centered around the PMT offset. An example of this is shown in Figure 8.

By finding the edges of the distribution in Figure 8, one can find the center and therefore the PMT offset. These are in Table 3 below (in channels).

Left bar	PMT offset (channels)	Right bar	PMT offset (channels)
0	20	18	-90
1	-12	19	-86
2	70	20	-62
3	64	21	-142
4	77	22	77
5	0	23	67
6	66	24	132
7	12	25	-24
8	-19	26	110
9	-69	27	74
10	-17	28	-15
11	-6	29	73
12	-1	30	0
13	85	31	-19
14	-56	32	-155
15	49	33	-45
16	19	34	-50
17	-8	35	110

Table 3: PMT offset (channels) for each of the time of flight detectors.

4.3.4 Results for TDC offsets

Using equations (15) and (14), the $(\text{TDC})^i_{t(b)}$ for each PMT can be found from r^i_{offset}, g_{offset} and PMT offsets. The global offset changed during August 2012, causing there to be two sets of offsets. The TDC offset results for Spring 2012 and shown in Table 4, and the results for Fall 2012 are shown in Tables 5. Because the global offsets need to be recalculated, these offsets will change slightly after tracking is finished.

ToF	Top (channels)	Bottom (channels)	ToF	Top (channels)	Bottom (channels)
0	-903.278	-923.278	18	-1009.36	-919.362
1	-1023.68	-1011.68	19	-1039.7	-953.705
2	-869.46	-939.46	20	-1013.52	-951.522
3	-978.926	-1042.93	21	-1013.35	-871.352
4	-928.572	-1005.57	22	-1074.31	-1151.31
5	-1032.29	-1032.29	23	-1049.39	-1116.39
6	-933.419	-999.419	24	-1012.42	-1144.42
7	-1029.26	-1041.26	25	-1056.82	-1032.82
8	-1020.62	-1001.62	26	-933.915	-1043.91
9	-1066.29	-997.285	27	-1031.02	-1105.02
10	-1007.77	-990.773	28	-943.508	-928.508
11	-1055.04	-1049.04	29	-1028.98	-1101.98
12	-967.575	-966.575	30	-1004.18	-1004.18
13	-1043.89	-1128.89	31	-1060.19	-1041.19
14	-982.468	-926.468	32	-1101.71	-946.709
15	-945.17	-994.17	33	-1099.43	-1054.43
16	-1145.26	-1164.26	34	-1197.38	-1147.38
17	-1129.97	-1121.97	35	-1160.58	-1270.58

Table 4: Total TDC offsets for top and bottom PMTs (channels) for each of the time of flight detectors. This is for runs before August 2012

ToF	Top (channels)	Bottom (channels)	ToF	Top (channels)	Bottom (channels)
0	-463.278	-483.278	18	-569.362	-479.362
1	-583.676	-571.676	19	-599.705	-513.705
2	-429.46	-499.46	20	-573.522	-511.522
3	-538.926	-602.926	21	-573.352	-431.352
4	-488.572	-565.572	22	-634.31	-711.31
5	-592.29	-592.29	23	-609.389	-676.389
6	-493.419	-559.419	24	-572.424	-704.424
7	-589.259	-601.259	25	-616.825	-592.825
8	-580.622	-561.622	26	-493.915	-603.915
9	-626.285	-557.285	27	-591.02	-665.02
10	-567.773	-550.773	28	-503.508	-488.508
11	-615.037	-609.037	29	-588.983	-661.983
12	-527.575	-526.575	30	-564.181	-564.181
13	-603.893	-688.893	31	-620.192	-601.192
14	-542.468	-486.468	32	-661.709	-506.709
15	-505.17	-554.17	33	-659.426	-614.426
16	-705.26	-724.26	34	-757.385	-707.385
17	-689.967	-681.967	35	-720.578	-830.578

Table 5: Total TDC offsets for top and bottom PMTs (channels) for each of the time of flight detectors. This is for runs after August 2012

4.4 ADC Parameters

4.4.1 Pedestals

For most runs, the ADC offsets are stored in `TOF_PEDS` in the raw data file. The mean from the pedestal runs is taken as the offset and subtracted from all ADC values. For runs with no `TOF_PEDS`, generally from early in the data-taking process, the ADC offsets default to the values stored in the ToF `init` file. The `TOF_PEDS` are not a perfect measurement of the actual pedestal position, as can be seen in Figure 11, but are close enough.

The offsets can also be calculated for each run using the `tof_pedestal_factory` recipe. First, events in a ToF bar are selected for which both the top and bottom PMTs have a TDC value of 0. This is because hits that originate in neighboring beam bunches as the event bunches can be integrated into the ADC value even though the TDC will be outside of the regular "valid" range. These are visible in the left plot in Figure 11, and are more noticeable in PMTs with higher rates, as one would expect. There is no way to remove these events completely, but this cut reduces them. Then, a Gaussian distribution is fit to the left side of the pedestal peak, to further reduce the impact of the tail at higher ADCs due to the remaining events like this.

The sigma of this Gaussian fit is saved in the ToF `init` file and is used in the ToF digitization as the amount of electronic noise in events. It is applied to each PMT ADC independently after the discrimination simulation. The digitization results with this amount of electronic noise agree fairly well with the observed thresholds, discussed in section 4.4.4.

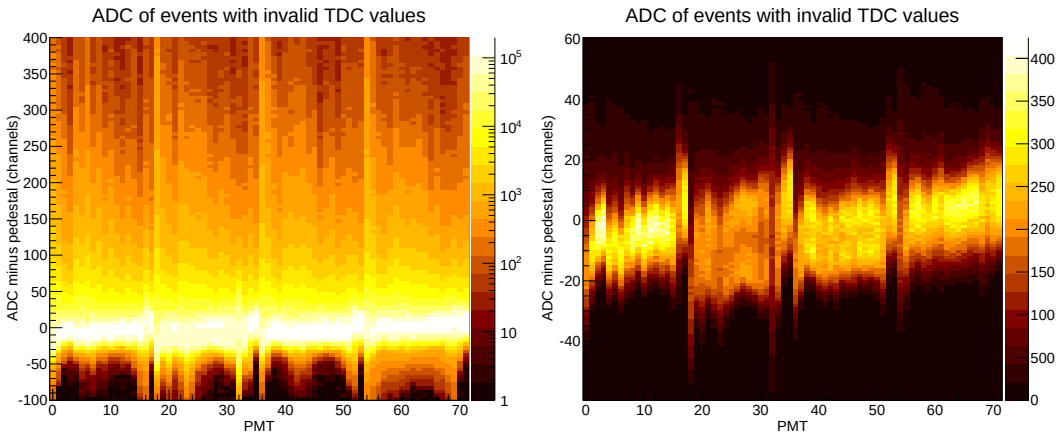

Figure 11: The ADC values for events with both TDCs invalid subtracted by the `TOF_PEDS` value of the pedestal. The left plot shows with a log scale the tail at high ADCs and the plot on the right shows a closeup of how the `TOF_PEDS`-subtracted pedestals are not centered exactly around zero. Since `TOF_PEDS` just records a mean value, it tends to overestimate the true pedestal ADC channel.

4.4.2 Gains

The gains for each PMT can be determined in a number of ways. Using the angle corrections mentioned in section 2.2, one can produce the dE/dx for cosmic muons in scintillator and thus calibrate the PMTs. Unfortunately, this is of limited use since the gains have drifted significantly between most of the data runs and the January cosmic runs. Having gains as a function of run number will eventually be necessary.

The energy distribution each bar should see in a normal data run is not easy to predict, even with an extensive Monte Carlo. Many of the features in the distribution do not come from elastic events. However, the top and bottom PMTs on a single bar should see the same event energies, before accounting for attenuation. This can be used to calculate the relative gain between a top and bottom PMT. To do this, all of the exact ADC values for one PMT were multiplied by some relative gain until the weighted sum of squares is minimized. With the relative gains matched, the f-factor (discussed in section 4.4.5) for a bar fluctuates around a value of 0.5. Thus, another equivalent approach is to just tune the relative gains until the calculated f-factors are all centered about 0.5. Plotting the f-factors for a bar as a function of reconstructed total event energy also reveals gain non-linearities in a way that is easy to see.

The absolute gains for each bar can also be extracted from data, by comparing to results from the Monte Carlo. One of the easiest ways to do this is by looking at the proton "sail plot," as illustrated in Figure 12. Since low energy protons deposit more energy in the scintillator, protons of various energies form a characteristic shape when looking at meantime vs energy deposition. This sail plot can be fitted to the MC calculation of the curve.

Finally, the most direct way of extracting the PMT gains from each run is by using tracking. Wire chamber data should allow a decent calculation of the position and angle of a track in the scintillator, allowing the calculation of dE/dx. In addition, the drift chamber data gives us information about the energy of the track and the particle ID.

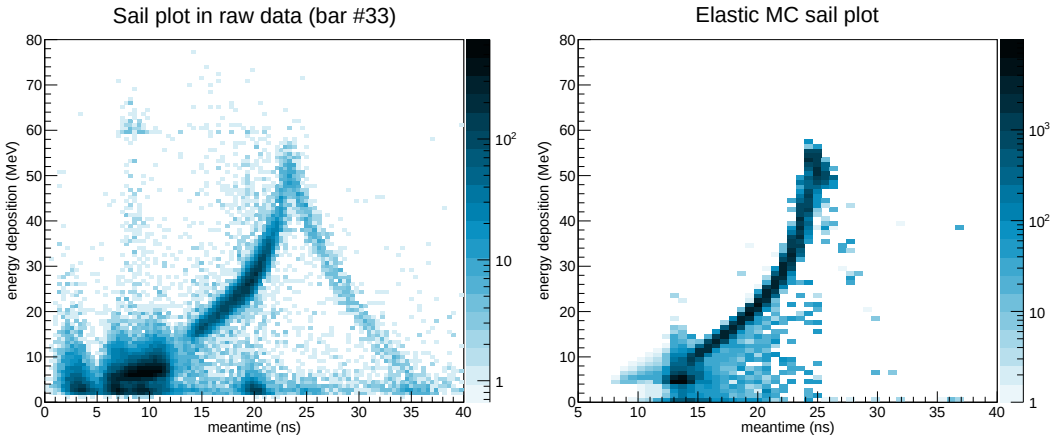

Figure 12: The broad proton "sail" seen in data (left) and the same plot as predicted for elastic events only in Monte Carlo (right.)

4.4.3 Attenuation

The attenuation length ℓ^i of a ToF bar is the approximate distance over which the magnitude of a signal will be reduced by a factor of $1/e$ when propagating. Due to age and wear on our scintillator, along with poor surface reflectivity, this attenuation is significant. Luckily, since we can calculate the vertical position from the TDC values, we can extract the approximate attenuation lengths for all of the ToF bars from data. This is done by plotting

$$\frac{G_b^i \left[\mathrm{ADC}\,{}_t^i - (\mathrm{ADC}_{\mathrm{ped}})_t^i\right]}{G_t^i \left[\mathrm{ADC}\,{}_b^i - (\mathrm{ADC}_{\mathrm{ped}})_b^i\right]} \approx e^{-2y^i/\ell^i} \tag{19}$$

as a function of y^i, and fitting the exponential to determine the constant (see Figure 13.)

These values are stored in the ToF `init` file and used to correct energy values in the data analysis and digitization following equations (6) and (7).

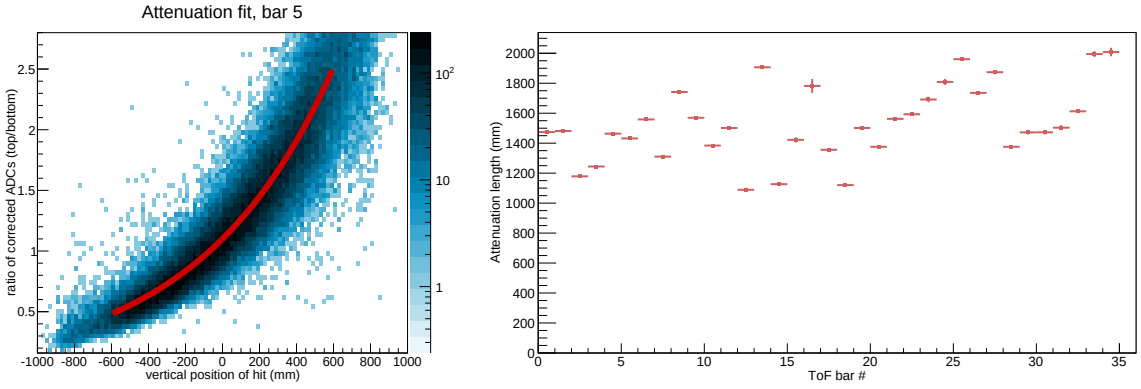

Figure 13: An example attenuation fit to data (left) and the attenuation values used in the ToF `init` file (right) from fitting to a broad sampling of data.

4.4.4 Thresholds

The ADC thresholds are only used in the digitization. They are extracted from the data for each PMT by taking the ADC distribution with a valid TDC and dividing it by the ADC distribution with a valid TDC or a valid TDC for the other PMT on the bar. This distribution, seen in Figure 14, is fit to a smeared step function:

$$\frac{\text{passing events}}{\text{all events}}(x) = \theta(x - x_t) * \frac{1}{\sigma\sqrt{2\pi}} e^{-x^2/2\sigma^2} = \frac{1}{2}\left[1 + \text{erf}\left(\frac{x - x_t}{2\sigma}\right)\right] \tag{20}$$

The threshold is then defined to be x_t, which is roughly the point in the step at which the ratio is 0.5. These values (combined from a large sample of data runs) are stored in the ToF `init` file and converted into an instantaneous threshold for use by the discrimination simulation by integrating Eq. (10) and dividing by the "integrated" threshold. These values are stored in pedestal-subtracted form, since it was found that they were most stable between runs this way.

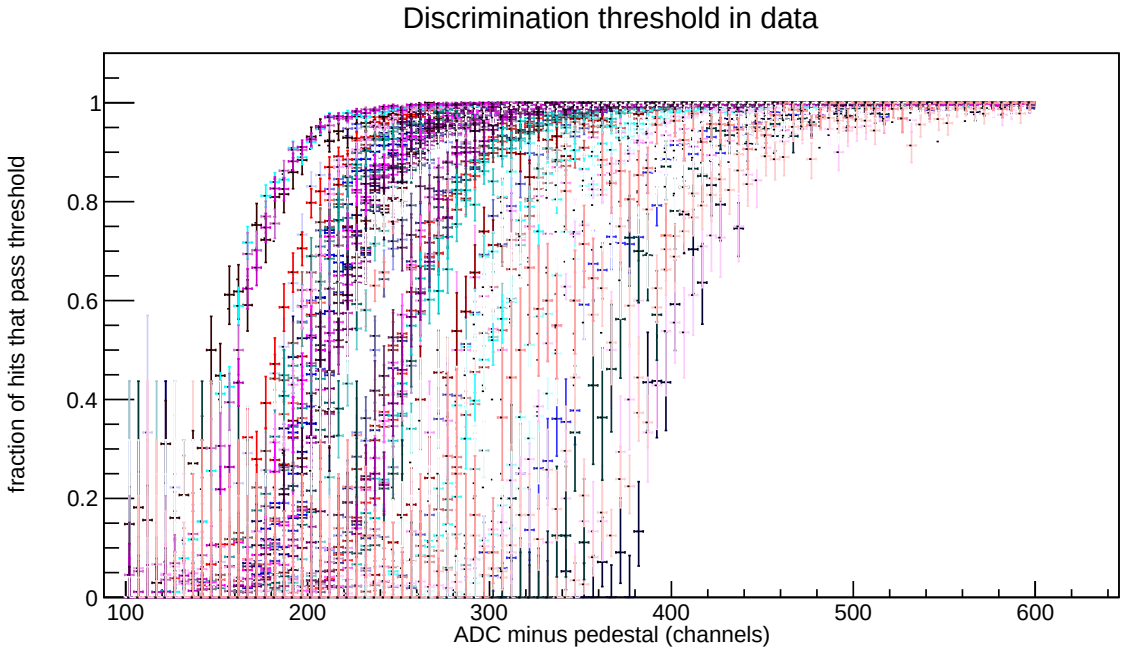

Figure 14: The threshold-passing distributions for all PMTs in a single run, illustrating that they each follow equation (20) quite well.

4.4.5 f-factors

The "f-factor" in equations (6) and (7) is designed to roughly take into account the fluctuation in how much light the two PMTs on a bar see relative to each other. If the gains of the two PMTs are correctly matched to each other, they will on average receive the same amount of light from a hit, after correcting for attenuation. The distribution of f-factors for a bar is Gaussian to good approximation. It is this Gaussian width that causes the thickness of the distribution seen in

Figure 13. When both ADCs in a hit are good (not overflowed) we can combine (6) and (7) to get

$$f^i = \left(1 + \frac{G_b^i \left[\mathrm{ADC}_t^i - (\mathrm{ADC}_{\mathrm{ped}})_t^i\right]}{G_t^i \left[\mathrm{ADC}_b^i - (\mathrm{ADC}_{\mathrm{ped}})_b^i\right]} e^{-2y^i/\ell^i}\right)^{-1} \tag{21}$$

to extract the f-factor distribution from the data. The width of these distributions varies from bar to bar, but remains fairly constant over time. The widths also vary with the amount of energy deposited in a bar. In order to store an f-factor rms for each bar that can be used in the digitization, we use an approximately energy-invariant quantity

$$\mathfrak{f} - \frac{1}{2} = \left(\frac{G_t^i + G_b^i}{2} \cdot E_{\mathrm{dep}}^i\right)^{-1/3} \left(f - \frac{1}{2}\right) \tag{22}$$

and store the rms values of this in the `init` file for use in the digitization. The inclusion of the $(G_t^i + G_b^i)/2$ factor is to reduce the sensitivity of the stored value to imperfect gain values. The strange energy dependence is not meaningful but is simply based on what is observed in the data in the relevant energy range. In the digitization, equation (22) is inverted to find σ_f for some particular hit energy deposition and used in equation (9) to calculate the amount of smearing needed (in combination with the noise on each PMT) to produce the appropriate observed $\sigma_{\mathfrak{f}}$.

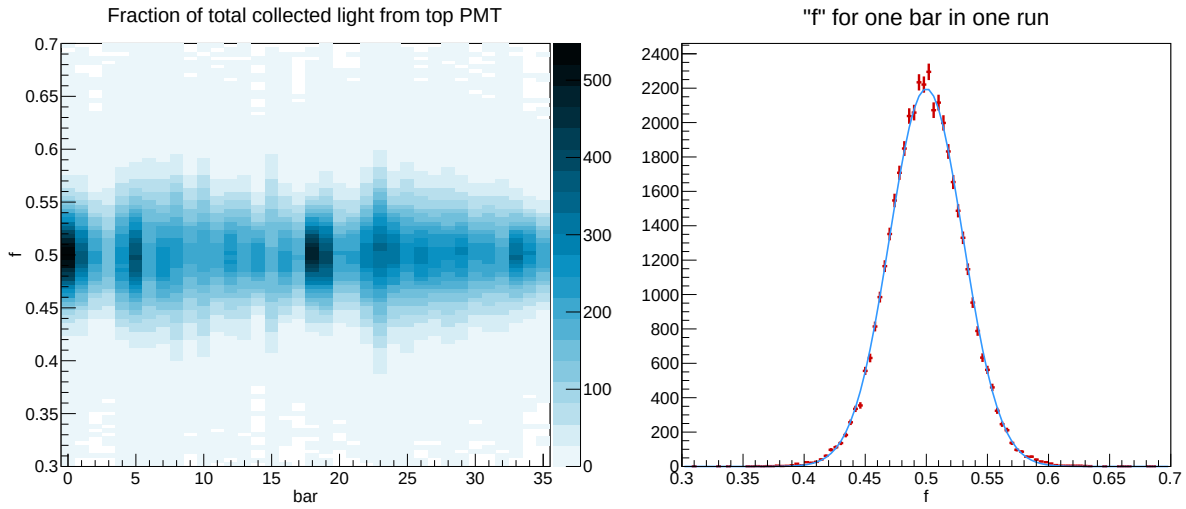

Figure 15: f-factor distributions in properly gain-matched data. The plot on the left shows the overall f-factor distribution (integrated over all hit energies) for each ToF bar. The plot on the right shows a sample fit from one bar to a Gaussian distribution.

5 Future Work

Upon the completion of the drift chamber tracking, several of the calibration and efficiency studies can be improved. Tracking will allow us to improve the calibrations of the global TDC offset (section 4.3.2) and the PMT gains (section 4.4.2). It will also allow for better parameterization

of the signals from the PMTs in the discrimination simulation (section 3.2.1) in the digitization routines. For the efficiency studies, tracking gives decent positional resolution for the ToF hits allowing us to further calibrate efficiencies near the edges of the paddles, where the SiPM studies miss.

Now that the ToF analysis and digitization software is operational, further analysis using the ToF detectors, including developing a ToF-based particle identification method, can be started. The energy deposited in a ToF hit gives insight into whether the particle was a minimally-ionizing particle, helping to discriminate between the leptons and protons. Depending on the accuracy of the time of flight, along with the momentum determination and the path length from the drift chambers, we may also reconstruct the mass of the particles from an interaction. An additional particle identification algorithm can be developed using the energy deposited and meantime from the ToF detectors with the momentum from the drift chambers.

References

[1] D. Hasell et al. OLYMPUS technical design report. Technical report, DESY, 2010.

[2] J. Howe. Concept art for The Lord of the Rings: Barad-dûr. `http://www.john-howe.com/portfolio/gallery/details.php?image_id=4699`, 1999.